Research Article

The Flow Separation of Peristaltic Transport for Maxwell Fluid between Two Coaxial Tubes

S. Z. A. Husseny,[1,2] Y. Abd elmaboud,[3,4] and Kh. S. Mekheimer[2]

[1] *Mathematical Department, Faculty of Science, King Abdulaziz University, Jeddah 21589, Saudi Arabia*

[2] *Mathematics Department, Faculty of Science, Al-Azhar University, Nasr City, Cairo 11884, Egypt*

[3] *Mathematics Department, Faculty of Science and Arts, King Abdulaziz University (KAU), Khulais 21921, Saudi Arabia*

[4] *Mathematics Department, Faculty of Science, Al-Azhar University (Assiut Branch), Assiut 71524, Egypt*

Correspondence should be addressed to Y. Abd elmaboud; yass_math@yahoo.com

We study the peristaltic mechanism of an incompressible non-Newtonian biofluid (namely, Maxwell model) in the annular region between two coaxial tubes. The inner tube represents the endoscope tube. The system of the governing nonlinear PDE is solved by using the perturbation method to the first order in dimensionless wavenumber. The modified Newton-Raphson method is used to predict the flow separation points along the peristaltic wall and the endoscope tube. The results show that the presence of the endoscope (catheter) tube in the artery increases the pressure gradient and shear stress. Such a result seems too reasonable from the physical and medical point of view.

1. Introduction

Peristalsis is produced by sequential waves of contractions in an elastic channel (tube), which push their fluid forward. In the urinary system, peristaltic movement is due to spontaneous muscular contractions of the ureteral wall which drives urine from the kidneys to the bladder through the ureters. Peristalsis is an important property of many biological systems which transports biofluids by its propulsive movements. It is responsible for the movement of chyme in the gastrointestinal tract, intrauterine fluid motion, vasomotion of the small blood vessels and in many glandular ducts. A number of analytical studies of peristaltic flows of different fluids have been reported [1–5].

Non-Newtonian fluids have wide-range applications, so they receive a great attention from scientists. The flows of non-Newtonian fluids are important because of their technological significance. Moreover, physiological flows indicate that non-Newtonian viscoelastic rheology is the correct way of properly describing the peristaltic flow through channels and tubes. Among many models, which have been employed to describe the non-Newtonian behavior exhibited by certain real fluids, Oldroyd fluid has obtained a special status; it includes elastic and memory effects exhibited by dilute solutions. Oldroyd fluid has been extensively used in many applications, and also results of simulations fit experimental data quite well [6, 7].

Recently, peristaltic motion of non-Newtonian fluids has been an important subject in the field of chemical, biomedical, and environmental engineering and science. A considerable amount of the literature has been reported [8–17].

Endoscope and catheters are very important tools for medical diagnosis and they have many clinical applications. The endoscope now is a very important tool used for determining the real causes responsible for many problems in the human organs through which the fluids are transported by peristaltic pumping such as, stomach and small intestine. Also from the fluid dynamic point of view, there is no difference between an endoscope and catheter. In medicine, a catheter is a tube that can be inserted into a body cavity, duct, or vessel. Catheters thereby allow drainage or injection of fluids. The process of inserting a catheter is called catheterization. Also, the insertion of an endoscope (catheter)

in an artery will alter the flow field and modify the pressure distribution. There are several investigations that studied the effect of an endoscope on peristaltic transport for different fluids [18–22].

So far, no attempt has been made to understand the effect of endoscope on the peristaltic motion for the Maxwell model which is a subclass of Oldroyd model. Therefore the main purpose of the present paper is to study the mathematical modeling of peristaltic transport of flow in a gap between two coaxial tubes, filled with an incompressible non-Newtonian fluid (Maxwell model). The inner tube is rigid (endoscope) and the outer one has wave trains moving independently. In this paper, we are concerned with viscoelastic flows governed by the Maxwell model. The mathematical modeling of this problem is explained below in brief.

2. Basic Equations

The basic equations governing the motion of Oldroyd fluid take the form

$$\nabla \cdot \mathbf{V}' = 0,$$
$$\rho \frac{D\mathbf{V}'}{Dt} = \nabla \cdot \mathbf{T}',$$
(1)

where ρ is the density, $\mathbf{V}'$ is the velocity vector, D/Dt denotes the material derivative, and $\mathbf{T}'$ is the Cauchy stress tensor. The Cauchy stress $\mathbf{T}'$ for an incompressible Oldroyd fluid can be expressed as

$$\mathbf{T}' = -p'\mathbf{I} + \mathbf{S}',$$
$$\mathbf{S}' + \Gamma \left(\frac{d\mathbf{S}'}{dt} - \mathbf{L}'\mathbf{S}' - \mathbf{S}'\mathbf{L}'^T \right)$$
$$= \mu \left[\mathbf{A}'_1 + \nu \left(\frac{d\mathbf{A}'_1}{dt} - \mathbf{L}'\mathbf{A}'_1 - \mathbf{A}'_1\mathbf{L}'^T \right) \right],$$
(2)

where p' is the pressure, μ is the coefficient of viscosity, $\mathbf{S}'$ is the extra stress, Γ is the relaxation time, and ν is the retardation time. The Rivlin-Ericksen tensors are defined as

$$\mathbf{A}'_1 = \left(\nabla \mathbf{V}' \right) + \left(\nabla \mathbf{V}' \right)^T, \qquad \mathbf{L}' = \nabla \mathbf{V}'.$$
(3)

It is worth mentioning that this model includes the Maxwell model for $\nu = 0$ and the classical linear case for $\Gamma = \nu = 0$.

3. Formulation of the Problem and Mathematical Model

In this paper, the flow of the Maxwell fluid is considered through the gap between coaxial tubes. The inner tube is rigid and the outer has a sinusoidal wave traveling down its walls. The geometry of the walls surface (Figure 1) is

$$R'_1 = a_1,$$
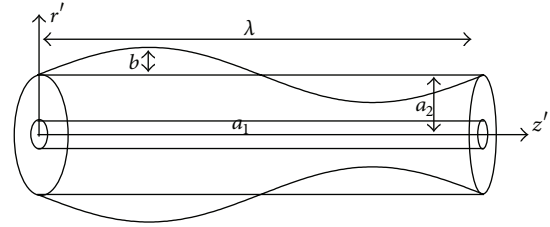$$R'_2 = a_2 + b \sin \left(\frac{2\pi}{\lambda} \left(Z' - ct' \right) \right),$$
(4)

Figure 1: Geometry of the problem.

where a_1 is the radius of the inner tube, a_2 is the radius of the outer tube at any axial distance Z', and b is the amplitude of the wave. Introducing a wave frame (r', z') moving with velocity c away from the fixed frame (R', Z') by the transformation

$$z' = Z' - ct', \qquad r' = R',$$
$$w' = W' - c, \qquad u' = U',$$
(5)

where (u', w') and (U', W') are the velocity components in the wave and fixed frame, respectively. After using this transformation then the mathematical formulation of this problem results in the following differential equations:

$$\frac{\partial u'}{\partial r'} + \frac{\partial w'}{\partial z'} + \frac{u'}{r'} = 0,$$

$$\rho \left[u' \frac{\partial u'}{\partial r'} + w' \frac{\partial u'}{\partial z'} \right] = -\frac{\partial p'}{\partial r'}$$
$$- \left[\frac{1}{r'} \frac{\partial}{\partial r'} \left(r' S'_{11} \right) - \frac{S'_{22}}{r'} + \frac{\partial S'_{13}}{\partial z'} \right],$$

$$\rho \left[u' \frac{\partial w'}{\partial r'} + w' \frac{\partial w'}{\partial z'} \right] = -\frac{\partial p'}{\partial z'} - \left[\frac{1}{r'} \frac{\partial}{\partial r'} \left(r' S'_{13} \right) + \frac{\partial S'_{33}}{\partial z'} \right].$$
(6)

The constitutive equations of Maxwell fluid are

$$S'_{11} + \Gamma \left[u' \frac{\partial S'_{11}}{\partial r'} + w' \frac{\partial S'_{11}}{\partial z'} - 2S'_{11} \frac{\partial u'}{\partial r'} - 2S'_{13} \frac{\partial u'}{\partial z'} \right] = -\mu \dot{\gamma}'_{11},$$

$$S'_{13} + \Gamma \left[u' \frac{\partial S'_{13}}{\partial r'} + w' \frac{\partial S'_{13}}{\partial z'} - S'_{33} \frac{\partial u'}{\partial z'} - S'_{11} \frac{\partial w'}{\partial r'} + \frac{u'}{r'} S'_{13} \right]$$
$$= -\mu \dot{\gamma}'_{13},$$

$$S'_{22} + \Gamma \left[u' \frac{\partial S'_{22}}{\partial r'} + w' \frac{\partial S'_{22}}{\partial z'} - \frac{2u'}{r} S'_{22} \right] = -\mu \dot{\gamma}'_{22},$$

$$S'_{33} + \Gamma \left[u' \frac{\partial S'_{33}}{\partial r'} + w' \frac{\partial S'_{33}}{\partial z'} - 2S'_{33} \frac{\partial w'}{\partial z'} - 2S'_{13} \frac{\partial w'}{\partial r'} \right]$$
$$= -\mu \dot{\gamma}'_{33},$$
(7)

where ρ is the density, P' is the pressure, S'_{ij} are the components of the extra stress tensor and $\dot{\gamma}'_{ij}$ are the components

of strain-rate tensor, and Γ is the relaxation time. The system of nonlinear differential equations has to be solved with the following boundary conditions:

$$w' = -c, \quad u' = 0, \quad \text{at } r' = r_1',$$
$$w' = -c, \quad u' = -c\frac{dr_2'}{dz'}, \quad \text{at } r' = r_2'. \tag{8}$$

Consider the following nondimensional variables and parameters:

$$r = \frac{r'}{a_2}, \qquad z = \frac{z'}{\lambda}, \qquad w = \frac{w'}{c},$$

$$u = \frac{\lambda u'}{a_2 c}, \qquad p = \frac{a_2^2}{\lambda \mu c} p', \qquad r_1 = \frac{r_1'}{a_2} = \epsilon, \qquad \phi = \frac{b}{a_2},$$

$$S_{ij} = \frac{a_2 S_{ij}'}{c\mu}, \qquad r_2 = \frac{r_2'}{a_2} = 1 + \phi \sin(2\pi z),$$

$$\text{Re} = \frac{\rho c a_2}{\mu}, \qquad \delta = \frac{a_2}{\lambda}, \qquad \epsilon = \frac{a_1}{a_2}, \qquad \text{Wi} = \frac{c\Gamma}{a_2}, \tag{9}$$

where ϕ is the amplitude ratio, Re is the Reynolds number, δ is the dimensionless wave number and Wi is the Weissenberg number, and ϵ is the radius ratio (the ratio between the radius of the inner tube and the radius of the outer). To proceed, we nondimensionalize ((4), (6)–(7)); this yields

$$r_1 = \epsilon, \tag{10}$$

$$r_2 = 1 + \phi \sin(2\pi z), \tag{11}$$

$$\frac{1}{r}\frac{\partial}{\partial r}(ru) + \frac{\partial w}{\partial z} = 0, \tag{12}$$

$$\text{Re}\,\delta^3 \left[u\frac{\partial u}{\partial r} + w\frac{\partial u}{\partial z} \right]$$
$$= -\frac{\partial p}{\partial r} - \delta \left[\frac{1}{r}\frac{\partial}{\partial r}(rS_{11}) - \frac{S_{22}}{r} + \delta\frac{\partial S_{13}}{\partial z} \right], \tag{13}$$

$$\text{Re}\,\delta \left[u\frac{\partial w}{\partial r} + w\frac{\partial w}{\partial z} \right] = -\frac{\partial p}{\partial z}$$
$$- \left[\frac{1}{r}\frac{\partial}{\partial r}(rS_{13}) + \delta\frac{\partial S_{33}}{\partial z} \right], \tag{14}$$

$$S_{11} + \text{Wi}\delta \left[u\frac{\partial S_{11}}{\partial r} + w\frac{\partial S_{11}}{\partial z} - 2S_{11}\frac{\partial u}{\partial r} - 2\delta S_{13}\frac{\partial u}{\partial z} \right]$$
$$= -2\delta\frac{\partial u}{\partial r}, \tag{15}$$

$$S_{13} + \text{Wi} \left[\delta \left(u\frac{\partial S_{13}}{\partial r} + w\frac{\partial S_{13}}{\partial z} - \delta S_{33}\frac{\partial u}{\partial z} + \frac{u}{r}S_{13} \right) - S_{11}\frac{\partial w}{\partial r} \right]$$
$$= -\left(\delta^2\frac{\partial u}{\partial z} + \frac{\partial w}{\partial r} \right), \tag{16}$$

$$S_{22} + \text{Wi}\delta \left[u\frac{\partial S_{22}}{\partial r} + w\frac{\partial S_{22}}{\partial z} - \frac{2u}{r}S_{22} \right] = -2\delta\frac{u}{r}, \tag{17}$$

$$S_{33} + \text{Wi} \left[\delta \left(u\frac{\partial S_{33}}{\partial r} + w\frac{\partial S_{33}}{\partial z} - 2S_{33}\frac{\partial w}{\partial z} \right) - 2S_{13}\frac{\partial w}{\partial r} \right]$$
$$= -2\delta \left(\frac{\partial w}{\partial z} \right). \tag{18}$$

The non-dimensional boundary conditions will be

$$w = -1, \quad u = 0, \quad \text{at } r = \epsilon,$$
$$w = -1, \quad u = -\frac{dr_2}{dz}, \quad \text{at } r = r_2. \tag{19}$$

4. Rate of Volume Flow in the Annulus

The instantaneous volume flow rate in the fixed frame is given by

$$Q = 2\pi \int_{R_1'}^{R_2'} R'W'\,dR', \tag{20}$$

where R_2' is a function of Z', t'. The rate of volume flow in the wave frame is given by

$$q = 2\pi \int_{r_1'}^{r_2'} r'w'\,dr', \tag{21}$$

where r_2' is a function of z' only. If we substitute (5) into (20) and make use of (21), we find that the two rates of volume flow are related through

$$Q = q + \pi c \left(r_2'^2 - r_1'^2 \right). \tag{22}$$

The time mean flow over a period T at a fixed position Z' is defined as

$$Q' = \frac{1}{T}\int_0^T Q\,dt. \tag{23}$$

Substituting (22) into (23) and integrating, we get

$$Q' = q + \pi c a_2^2 \left(1 + \frac{\phi^2}{2} \right) - \pi c r_1'^2. \tag{24}$$

On defining the dimensionless time-mean flows $\overline{Q}$ and F, respectively, in the fixed and wave frame as

$$\overline{Q} = \frac{Q'}{\pi c a_2^2}, \qquad F = \frac{q}{\pi c a_2^2}, \tag{25}$$

one finds that (24) may be written as

$$\overline{Q} = F + 1 + \frac{\phi^2}{2} - \epsilon^2, \tag{26}$$

where

$$F = 2 \int_{r_1}^{r_2} rw \, dr. \tag{27}$$

5. Perturbation Solution

It is evident that ((12)–(18)) are highly nonlinear, and, as such, it is not possible to obtain the solutions in a closed form. In order to solve the present problem, we expanded the flow quantities in a power series of the small parameter δ as follows:

$$u = u_0 + \delta u_1 + \delta^2 u_2 + \cdots,$$

$$w = w_0 + \delta w_1 + \delta^2 w_2 + \cdots,$$

$$p = p_0 + \delta p_1 + \delta^2 p_2 + \cdots, \tag{28}$$

$$\tau_{ij} = S_{ij}^{(0)} + \delta S_{ij}^{(1)} + \delta^2 S_{ij}^{(2)} + \cdots \quad \text{where } i, j = 1, 2, 3,$$

$$F = F_0 + \delta F_1 + \delta^2 F_2 + \cdots.$$

If we substitute (28) into ((12)–(19)) and separate the terms of different order in δ, we obtain the following systems of partial differential equations together with boundary conditions as follows.

System of Order Zero. Consider

$$0 = -\frac{\partial p_0}{\partial r},$$

$$0 = -\frac{\partial p_0}{\partial z} - \left(\frac{1}{r} \frac{\partial}{\partial r} \left(r S_{13}^0 \right) \right),$$

$$S_{11}^0 = 0,$$

$$S_{13}^0 + \text{Wi} \left(-S_{11}^0 \frac{\partial w_0}{\partial r} \right) = -\frac{\partial w_0}{\partial r},$$

$$S_{22}^0 = 0,$$

$$S_{33}^0 + \text{Wi} \left(-2S_{13}^0 \frac{\partial w_0}{\partial r} \right) = 0, \tag{29}$$

with the boundary conditions:

$$w_0 = -1, \quad u_0 = 0, \quad \text{at } r = r_1 = \epsilon,$$

$$w_0 = -1, \quad u_0 = -\frac{dr_2}{dz}, \quad \text{at } r = r_2. \tag{30}$$

System of Order One. Consider

$$0 = -\frac{\partial p_1}{\partial r} - \frac{1}{r} \frac{\partial}{\partial r} \left(r S_{11}^0 \right) - \frac{1}{r} S_{22}^0,$$

$$\text{Re} \left[u_0 \frac{\partial w_0}{\partial r} + w_0 \frac{\partial w_0}{\partial z} \right] = -\frac{\partial p_1}{\partial z} - \left(\frac{1}{r} \frac{\partial}{\partial r} \left(r S_{13}^1 \right) \right) + \frac{\partial S_{33}^0}{\partial z},$$

$$S_{11}^1 + \text{Wi} \left(u_0 \frac{\partial S_{11}^0}{\partial r} + w_0 \frac{\partial S_{11}^0}{\partial z} - 2 S_{11}^0 \frac{\partial u_0}{\partial r} \right) = -2 \frac{\partial u_0}{\partial r},$$

$$S_{13}^1 + \text{Wi} \left[u_0 \frac{\partial S_{13}^0}{\partial r} + w_0 \frac{\partial S_{13}^0}{\partial z} + \frac{u_0}{r} S_{13}^0 - S_{11}^0 \frac{\partial w_1}{\partial r} - S_{11}^1 \frac{\partial w_0}{\partial r} \right]$$

$$= -\frac{\partial w_1}{\partial r},$$

$$S_{22}^1 + \text{Wi} \left[u_0 \frac{\partial S_{22}^0}{\partial r} + w_0 \frac{\partial S_{22}^0}{\partial z} - \frac{2u_0}{r} S_{22}^0 \right] = -2 \frac{u_0}{r},$$

$$S_{33}^1 + \text{Wi} \left[u_0 \frac{\partial S_{33}^0}{\partial r} + w_0 \frac{\partial S_{33}^0}{\partial z} - 2 S_{33}^0 \frac{\partial w_0}{\partial z} \right.$$

$$\left. - 2 S_{13}^0 \frac{\partial w_1}{\partial r} - 2 S_{13}^1 \frac{\partial w_0}{\partial r} \right] = -2 \frac{\partial w_0}{\partial z}, \tag{31}$$

with the boundary conditions:

$$w_1 = 0, \quad u_1 = 0, \quad \text{at } r = r_1 = \epsilon,$$

$$w_1 = 0, \quad u_1 = 0, \quad \text{at } r = r_2. \tag{32}$$

Solving the above sets of equations with the corresponding boundary conditions, we get the following.

Zero-Order Problem. Consider

$$w_0(r, z) = -1 + \log[r] \Omega_7 + \Omega_8 + r^2 \Omega_9, \tag{33}$$

$$u_0(r, z) = \Omega_3 - r\Omega_4 + r \log[r] \Omega_5 - r\Omega_6, \tag{34}$$

$$\frac{dp_0}{dz} = \left(8 \left(F_0 - \epsilon^2 + r_2^2 \right) \left(\log[\epsilon] - \log[r_2] \right) \right)$$

$$\times \left(\left[\left(\epsilon^2 - r_2^2 \right) \left(-\epsilon^2 + r_2^2 + \epsilon^2 \log[\epsilon] + r_2^2 \log[\epsilon] \right. \right. \right.$$

$$\left. \left. \left. - \epsilon^2 \log[r_2] - r_2^2 \log[r_2] \right) \right] \right)^{-1}. \tag{35}$$

We point out that the zero order solution coincides with the solution obtained by Mekheimer and Abd elmaboud [22] and is still independent of the viscoelastic effects.

First-Order Problem. Substituting the zeroth-order solution ((33) and (34)) into the equation of motion obtained for first

order, one finds that the solution of the first-order problem will be in the form

$$
w_1(r,z) = \frac{dp_1}{dz}\left(\frac{r^2}{4} + \frac{\left(\epsilon^2/4 - r_2^2/4\right)\log[r]}{\log[r_2] - \log[\epsilon]}\right.
$$

$$
\left. + \frac{\epsilon^2 \log[r_2] - r_2^2 \log[\epsilon]}{4\left(\log[\epsilon] - \log[r_2]\right)}\right)
$$

$$
+ r^2\Omega_{17} + r^2\log[r]\,\Omega_{18}
$$

$$
+ r^4\left(\Omega_{19} + \log[r]\,\Omega_{20}\right) + \Omega_{21}
$$

$$
+ \log[r]\,\Omega_{22} + \frac{\Omega_{15} + 2\mathrm{Wi}\log[r]\,\Omega_5\Omega_7}{r}
$$

$$
+ \frac{2}{9}r^3\,\mathrm{Re}\,\Omega_3\Omega_9 + r\left(\Omega_{16} + 4\mathrm{Wi}\log[r]\,\Omega_5\Omega_9\right)
$$

$$
+ \frac{1}{4}r^2\,\mathrm{Re}\log[r]^2\Omega_7\Omega_7' + \frac{1}{2}\mathrm{Wi}\log[r]^2\Omega_7\Omega_7'
$$

$$
+ \frac{1}{36}r^6\,\mathrm{Re}\,\Omega_9\Omega_9',
$$

(36)

$$
u_1(r,z) = c_6
$$

$$
+ \frac{1}{r}\left\{-\frac{1}{36}r^6\left(6\Omega_{19}' - \Omega_{20}\right)\right.
$$

$$
- r\left(\Omega_{15}' - 2\mathrm{Wi}\left(\Omega_7\Omega_5' + \Omega_5\Omega_7'\right)\right)
$$

$$
- \frac{2}{45}r^5\,\mathrm{Re}\left(\Omega_9\Omega_3' + \Omega_3\Omega_9'\right)
$$

$$
- \frac{1}{9}r^3\left(3\Omega_{16}' - 4\mathrm{Wi}\left(\Omega_9\Omega_5' + \Omega_5\Omega_9'\right)\right)
$$

$$
- \frac{1}{16}r^2\left(r^2\,\mathrm{Re} + 4\mathrm{Wi}\right)\left(\log[r]\right)^2
$$

$$
\times\left(\Omega_7'^2 + \Omega_7\Omega_7''\right)
$$

$$
- \frac{1}{128}r^4\left(32\Omega_{17}' - 8\Omega_{18}'\right.
$$

$$
\left. + \mathrm{Re}\left(\Omega_7'^2 + \Omega_7\Omega_7''\right)\right)
$$

$$
- \frac{r^2}{\left(16r_2(\log[\epsilon] - \log[r_2])^2\right)}
$$

$$
\times\left(\frac{dp_1}{dz}r_2'\left(1 + 2\log[\epsilon]\right)\right.
$$

$$
\times\left(\epsilon^2 + r_2^2\left(2\log[r_2] - 1 - 2\log[\epsilon]\right)\right)
$$

$$
+ 2r_2(\log[\epsilon] - \log[r_2])^2
$$

$$
\left.\times\left(4\Omega_{21}' - 2\Omega_{22}' + \mathrm{Wi}\left(\Omega_7'^2 + \Omega_7\Omega_7''\right)\right)\right)
$$

$$
- \log[r]\left[\frac{1}{6}r^6\Omega_{20}'\right.
$$

$$
+ 2r\mathrm{Wi}\left(\Omega_7\Omega_5' + \Omega_5\Omega_7'\right)
$$

$$
+ \frac{4}{3}r^3\mathrm{Wi}\left(\Omega_9\Omega_5' + \Omega_5\Omega_9'\right)
$$

$$
+ \frac{1}{32}r^4\left(8\Omega_{18}' - \mathrm{Re}\left(\Omega_7'^2 + \Omega_7\Omega_7''\right)\right)
$$

$$
+ \frac{r^2}{\left(8r_2(\log[\epsilon] - \log[r_2])^2\right)}
$$

$$
\times\left(\frac{dp_1}{dz}r_2'\left(-\epsilon^2\right.\right.
$$

$$
+ r_2^2\left(1 + 2\log[\epsilon]\right.
$$

$$
\left.\left. -2\log[r_2]\right)\right)
$$

$$
+ 2r_2(\log[\epsilon] - \log[r_2])^2
$$

$$
\times\left(2\Omega_{22}'\right.
$$

$$
\left.\left.\left. - \mathrm{Wi}\left(\Omega_7'^2 + \Omega_7\Omega_7''\right)\right)\right)\right]
$$

$$
\left. - \frac{r^8\,\mathrm{Re}}{288}\left(\Omega_9'^2 + \Omega_9\Omega_9''\right)\right\},
$$

(37)

$$
\frac{dp_1}{dz} = 1\left(-\frac{\epsilon^4}{8} + \frac{\epsilon^4}{8\left(\log[\epsilon] - \log[r_2]\right)}\right.
$$

$$
- \frac{\epsilon^2 r_2^2}{4\left(\log[\epsilon] - \log[r_2]\right)}
$$

$$
\left. + \frac{r_2^4\left(1 + \log[\epsilon] - \log[r_2]\right)}{8\left(\log[\epsilon] - \log[r_2]\right)}\right)^{-1}
$$

$$
\times\left\{-F_1 - 2\epsilon\Omega_{15} - \frac{2}{3}\epsilon^3\Omega_{16} - \frac{1}{2}\epsilon^4\Omega_{17}\right.
$$

$$
+ \frac{1}{8}\epsilon^4\Omega_{18} - \frac{1}{2}\epsilon^4\log[\epsilon]\,\Omega_{18} - \frac{1}{3}\epsilon^6\Omega_{19}
$$

$$
+ \frac{1}{18}\epsilon^6\Omega_{20} - \frac{1}{3}\epsilon^6\log[\epsilon]\,\Omega_{20}
$$

$$
+ \frac{1}{18}r_2^6\left(6\Omega_{19} + \left(-1 + 6\log[r_2]\right)\Omega_{20}\right)
$$

$$
- \epsilon^2\Omega_{21} + \frac{1}{2}\epsilon^2\Omega_{22} - \epsilon^2\log[\epsilon]\,\Omega_{22}
$$

$$
+ 4\mathrm{Wi}\epsilon\Omega_5\Omega_7 - 4\mathrm{Wi}\epsilon\log[\epsilon]\,\Omega_5\Omega_7
$$

$$
+ 2r_2\left(\Omega_{15} + 2\mathrm{Wi}\left(-1 + \log[r_2]\right)\Omega_5\Omega_7\right)
$$

$$
- \frac{4}{45}\,\mathrm{Re}\,\epsilon^5\Omega_3\Omega_9 + \frac{4}{45}\,\mathrm{Re}\,r_2^5\Omega_3\Omega_9
$$

$$+ \frac{8}{9} \mathrm{Wi} \epsilon^3 \Omega_5 \Omega_9 - \frac{8}{3} \mathrm{Wi} \epsilon^3 \log [\epsilon] \, \Omega_5 \Omega_9$$

$$+ \frac{2}{9} r_2^3 \left(3 \Omega_{16} + 4 \mathrm{Wi} \left(-1 + 3 \log [r_2] \right) \Omega_5 \Omega_9 \right)$$

$$- \frac{1}{4} \mathrm{Wi} \epsilon^2 \Omega_7 \Omega_7' - \frac{1}{64} \mathrm{Re} \, \epsilon^4 \Omega_7 \Omega_7'$$

$$+ \frac{1}{2} \mathrm{Wi} \epsilon^2 \log [\epsilon] \, \Omega_7 \Omega_7'$$

$$+ \frac{1}{16} \mathrm{Re} \, \epsilon^4 \log [\epsilon] \, \Omega_7 \Omega_7'$$

$$- \frac{1}{2} \mathrm{Wi} \epsilon^2 \log [\epsilon]^2 \Omega_7 \Omega_7'$$

$$- \frac{1}{8} \mathrm{Re} \, \epsilon^4 \log [\epsilon]^2 \Omega_7 \Omega_7'$$

$$+ \frac{1}{4} r_2^2 \left(4 \Omega_{21} + \left(-2 + 4 \log [r_2] \right) \Omega_{22} \right.$$

$$+ \mathrm{Wi} \left(1 + 2 \left(-1 + \log [r_2] \right) \right.$$

$$\left. \times \log [r_2] \right) \Omega_7 \Omega_7' \right)$$

$$+ \frac{1}{64} r_2^4 \left(32 \Omega_{17} + 8 \left(-1 + 4 \log [r_2] \right) \Omega_{18} \right.$$

$$+ \mathrm{Re} \left(1 - 4 \log [r_2] \right.$$

$$\left. + 8 \log [r_2]^2 \right) \Omega_7 \Omega_7' \right)$$

$$\left. - \frac{1}{144} \mathrm{Re} \, \epsilon^8 \Omega_9 \Omega_9' + \frac{1}{144} \mathrm{Re} \, r_2^8 \Omega_9 \Omega_9' \right\}, \tag{38}$$

where $(')$ represents differentiation with respect to z, and the coefficients Ω_{ij} and c_6 that appear in the whole paper are listed in the appendix. The total expressions for the velocities and the pressure gradient up to first order can be obtained by substituting ((33)–(38)) and $F_0 = F - \delta F_1$ into (28) and neglecting the terms greater than $O(\delta)$.

The pressure rise Δp, in nondimensional form, is given by

$$\Delta p = \int_0^\Lambda \frac{dp}{dz} dz, \tag{39}$$

where $\Lambda = L/\lambda$.

The integral in (39) is not integrable in a closed form; it is evaluated numerically with aid of the MATHEMATICA programme.

6. The Flow Separation Points

In cases of separation from bodies of smooth geometrical form, the surface streamlines are observed to leave (separate) the surface more or less tangentially. In the case where the boundary layer is laminar, in sufficient momentum exchange takes, the flow is unable to adjust to the increasing pressure and separates from the surface. Contemplation of the velocity

field shows that it is plausible to identify the point of separation (z_s) on the walls with points where the circulation vanishes (the vorticity equal zero) [23]. A condition used to prognosticate the separation in boundary-layer theory is to set the vorticity equal to zero on the boundary walls [10], as

$$\eta_z = \frac{\partial u}{\partial z} - \frac{\partial w}{\partial r}, \quad \text{at } r = \epsilon, \ r_2 \tag{40}$$

(the result of (40) is omitted because of large output). We can solve the resultant equation ($\eta_z|_{r=r_2} = 0$ and $\eta_z|_{r=\epsilon} = 0$) numerically using the modified Newton-Raphson method [24] to get the flow separation points z_s. The flow separation points z_s with different values of the amplitude ratio ϕ in the tube ($\epsilon = 0$) and in the annulus ($\epsilon \neq 0$) are summarized in Table 1.

The table shows that there are two values of separation points z_s. An important point here is that there is no separation when $\phi = 0$ on the tube wall and on the annulus walls. Moreover, the separation points are different in tube than those in annulus. Also, the separation points are different from the amplitude ratio to the other one and from radius ratio to the other one. The effect of various parameters of interest on the wall vorticity will be discussed in the next section.

7. Numerical Results and Discussion

This section is divided into three subsections. In the first subsection, the effects of various parameters on the velocity distribution and wall vorticity are investigated. The pumping characteristics and shear stresses are discussed in the second subsection. The trapping phenomenon is illustrated in the last subsection. The emerging parameters of our analysis are the Reynolds number Re, wave number δ, the Weissenberg number Wi, the radius ratio ϵ, the amplitude ratio ϕ, and the average flow rate $\overline{Q}$. These have easy physical interpretations: δ is a measure of how large the semi depth of the peristaltic motion is, as compared to its wavelength. It is an aspect ratio and thus an expression of shallowness. The Reynolds number Re is formed with the wave speed, the amplitude, and the kinematic viscosity of the Newtonian part of the constitutive behavior. Wi measures the elastic contributions of the stress behavior. ϵ gives the ratio between the radius of the inner tube and the radius of the outer tube of the annulus. ϕ is a measure of how large the wave amplitude of the peristaltic wave is as compared to the radius of the outer tube.

7.1. Axial Velocity, Wall Vorticity, and Flow Separation. This subsection describes the influences of various emerging parameters of our analysis on the transverse distributions of the longitudinal velocity at the gap of the annulus $w(r, z)$ and the wall vorticity η_z on the outer and inner tube walls. Figures 2, 3, 4, 5, 6, 7, 8, and 9 display the effects of Re, δ, Wi, ϵ, ϕ, and $\overline{Q}$ on $w(r, z)$ and η_z. From Figures 2 and 3, owing to the limit of the no-slip boundary condition in (19), the velocity at wall tubes has the same value $w = -1$ in the wave frame for all values of the parameters; that is, the fluid velocity at the annulus walls moves with an opposite velocity to that of the

TABLE 1: Computed values of the flow separation points z_s for different values of amplitude ratio ϕ at $\overline{Q} = 1$, Re = 10, Wi = 0.01, and $\delta = 0.01$.

ϕ	Tube $\epsilon = 0$	Annulus $\epsilon = 0.05$	Annulus $\epsilon = 0.1$
	z_s	z_s	z_s
0	$\cdots$	$\cdots$	$\cdots$
	$\cdots$	$\cdots$	$\cdots$
0.1	0.6045724	0.6504434	0.6504434
	0.8975483	0.8702141	0.8615617
0.2	0.5678108	0.5987454	0.6078304
	0.9194012	0.9139087	0.9015790
0.3	0.5575255	0.5987454	0.6078304
	0.9102325	0.9076357	0.8959550
0.4	0.5479702	0.6050183	0.6162664
	0.9014732	0.9043910	0.8901146
0.5	0.5327034	0.5991780	0.6162664
	0.904884	0.9072031	0.8901146

FIGURE 2: The velocity distribution w, across the annulus with different values of Re and δ at $\epsilon = 0.01$, Wi = 0.01, $\overline{Q} = 1.5$, $\phi = 0.4$, and $z = 0.1$, where $r \in [\epsilon, r_2]$.

FIGURE 3: The velocity distribution w, across the annulus with different values of ϵ and Wi at Re = 3, $\delta = 0.1$, $\overline{Q} = 1.5$, $\phi = 0.4$, and $z = 0.1$, where $r \in [\epsilon, r_2]$.

wave that propagates on the outer wall of the annulus. As we expected, the magnitudes of forward and backward flows (in the annulus gap) increase when the wave number δ (i.e, small wave length for the peristaltic wave, so the amplitude of the wave increases) and Reynolds number Re increase. Moreover, Figure 2, indicates that the location of the reflux phenomenon in the flow depends upon the magnitudes of Re and δ. Effects of the Weissenberg number Wi and the radius ratio ϵ are illustrated in Figure 3. The curves for Wi match together and a slight difference occurs only for $\epsilon = 0.01$ near the inner wall. For $\epsilon = 0.1$ the data are identical for Wi values. It is worth mentioning that the shear stress decreases with an increase in the relaxation parameter Γ, Wi $= c\Gamma/a_2$, so that the velocity increases. However, an increase of the radius ratio ϵ produces a decrease of the velocity and more back flow occurs.

The variation of the flow vorticity at the outer and inner tubes along the annulus is illustrated in Figures 4–9 for different values of the emerging parameters. These figures show that the vorticity increases in the wider part of the annulus, $z \in (0, 0.5)$, while it decreases as going to the narrow part, $z\epsilon(0.51, 1)$, and separation occurs at the outer tube but at the inner one there are no separation points appearing (Figures 7–9). Moreover, the separation points positions are in the narrow part of the annulus. In solid annulus (no peristaltic $\phi = 0$,) we observe that the vorticity is constant along the annulus and, therefore, there are no separation points (this result is compatible with the results in Table 1.). By increasing the value of the amplitude ratio ϕ (peristaltic transport), separation points appear but this depends on the position z.

7.2. The Pumping Characteristics and Shear Stresses. This subsection describes the influences of various emerging parameters of our analysis on the axial pressure gradient (dp/dz), the pressure rise per wavelength (Δp), and the shear stresses at the annulus walls. The effects of these parameters are shown in Figures 10, 11, 12, 13, 14, 15, and 16. Figures 10 and 11 illustrate that in the wider part of the channel
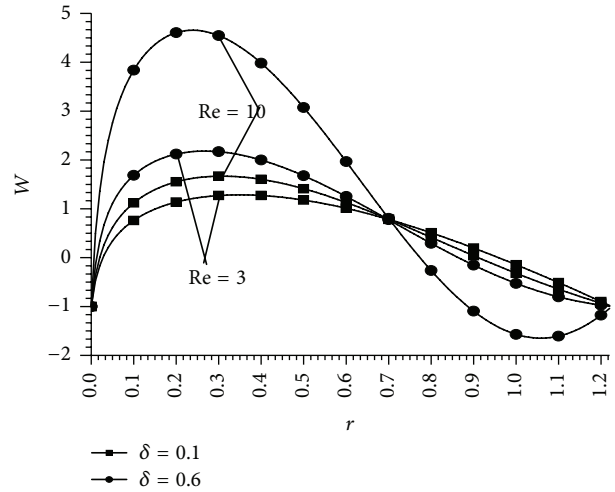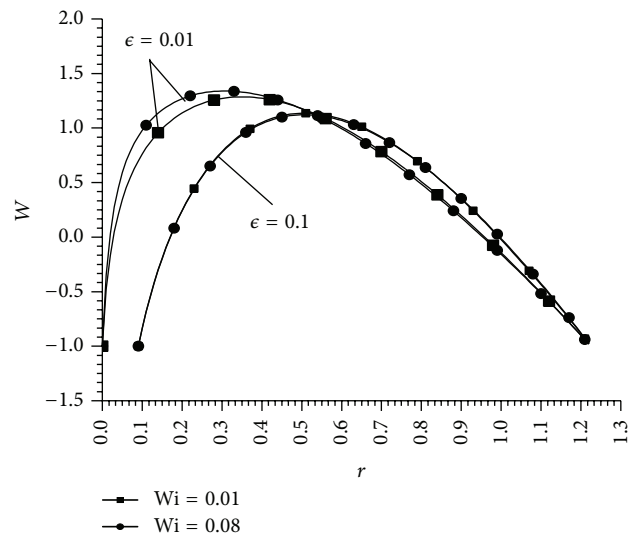
$z \in [0, 0.6]$ and $[0.9, 1.0]$ the pressure gradient is relatively small; that is, the flow can easily pass without imposition of large pressure gradient. However, in a narrow part of the channel $z \in [0.6, 0.9]$ a much larger pressure gradient is required to maintain the same flux to pass it, especially for the narrowest position near $z = 0.8$. This is in good agreement with the physical situation. Also from these two figures we observe the effect of ϵ and δ on the pressure gradient, for fixed values of the other parameters, where the amplitude of dp/dx increases with increasing ϵ and δ. Figure 11 shows that the amplitude of the axial pressure gradient decreases as Reynolds number increases. Reynolds number is the ratio of inertial to viscous forces and with the increase of Reynolds number the viscous forces decrease so the velocity increases
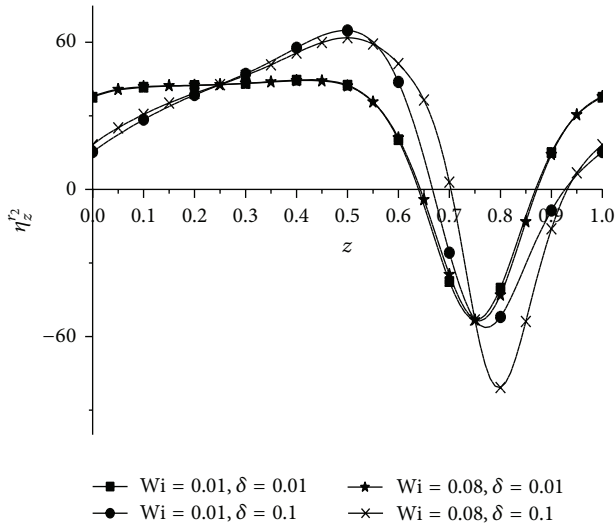
FIGURE 4: Variation of wall vorticity η_z^{r2} versus z with different values of δ and Wi at Re $= 5$, $\epsilon = 0.01$, $\overline{Q} = 1.5$, and $\phi = 0.4$.
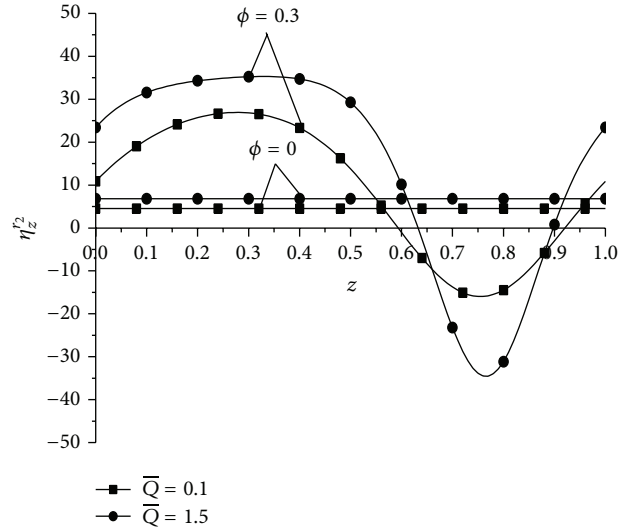
FIGURE 6: Variation of wall vorticity η_z^{r2} versus z with different values of $\overline{Q}$ and ϕ at Wi $= 0.02$, $\delta = 0.1$, $\epsilon = 0.01$, and Re $= 1$.
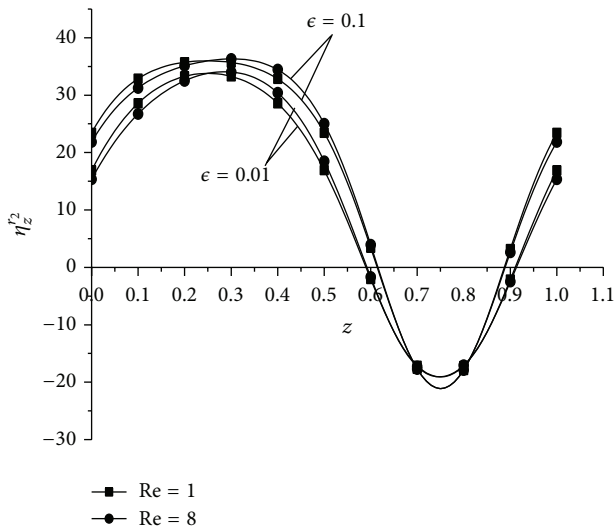
FIGURE 5: Variation of wall vorticity η_z^{r2} versus z with different values of ϵ and Re at Wi $= 0.01$, $\delta = 0.1$, $\overline{Q} = 1$, and $\phi = 0.4$.
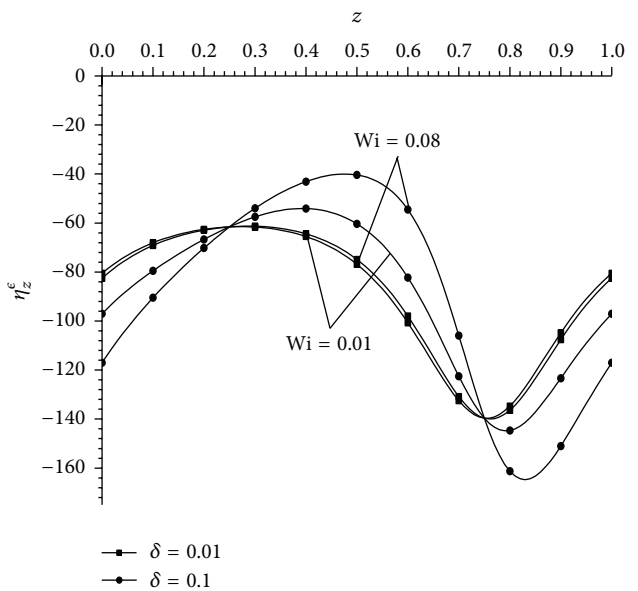
FIGURE 7: Variation of wall vorticity η_z^{ϵ} versus z with different values of δ and Wi at Re $= 5$, $\epsilon = 0.01$, $\overline{Q} = 1.5$, and $\phi = 0.4$.

and so the pressure gradient decreases. Also, as the Wi increases (stresses decreases) the pressure gradient increases. In Figure 12, the pressure rise Δp is illustrated in terms of the wave amplitude ϕ of the wall disturbance with various values of the radius ratio ϵ. Firstly, it is obvious that with increasing occlusion ϕ the pressure drop increases; that is, an increase of the pressure gradient is needed to push the same flux to pass the gap annulus. Secondly, the pressure rise for an annulus is higher than that for a tube. Figure 12 is sectored so that the upper right-hand quadrant denotes the region of peristaltic pumping where $\overline{Q} > 0$ (positive pumping) and $\Delta p > 0$ (adverse pressure gradient). The lower right-hand quadrant denotes the region of augmented pumping where $\overline{Q} > 0$ (positive pumping) and $\Delta p < 0$ (favorable

pressure gradient) and the upper left-hand quadrant denotes the region of retrograde pumping (or backward pumping) where $\overline{Q} < 0$ and $\Delta p > 0$ (adverse pressure gradient); in this region the flows is opposite to the direction of the peristaltic motion. It is clear that the peristaltic pumping region becomes wider as the radius ratio ϵ, amplitude ratio ϕ (the ratio between wave amplitude and the radius of the outer tube), increases.

The influences of various parameters of our analysis on shear stress τ_{13} at the outer and inner walls are shown in Figures 13–16. The shear stress τ_{13} in the outer tube varies along the annulus from small value in the wider part to large
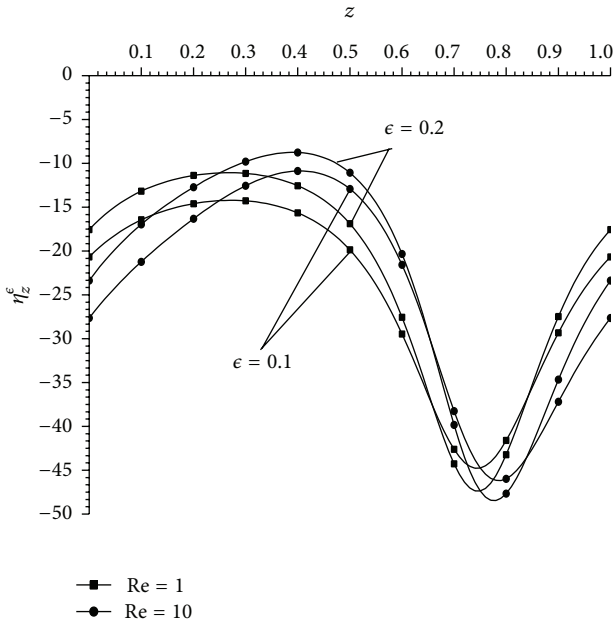
FIGURE 8: Variation of wall vorticity η_z^ϵ versus z with different values of ϵ and Re at Wi $= 0.01$, $\delta = 0.1$, $\overline{Q} = 1$, and $\phi = 0.4$.
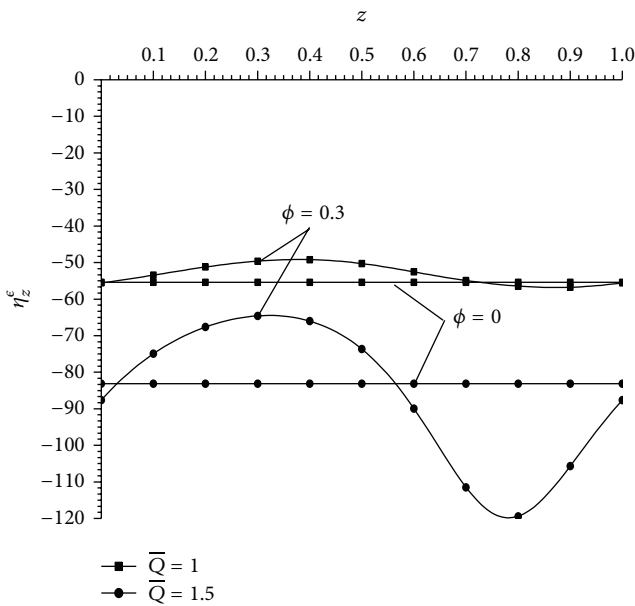
FIGURE 9: Variation of wall vorticity η_z^ϵ versus z with different values of $\overline{Q}$ and ϕ at Wi $= 0.02$, $\delta = 0.1$, $\epsilon = 0.01$, and Re $= 1$.

FIGURE 10: Variation of pressure gradient versus z with different values of δ and ϵ at Wi $= 0.05$, $\overline{Q} = 0.5$, $\phi = 0.4$, and Re $= 2$.

FIGURE 11: Variation of pressure gradient versus z with different values of Wi and Re at $\delta = 0.1$, $\overline{Q} = 0.1$, $\phi = 0.4$, and $\epsilon = 0.1$.

value in the narrow part but the shear stress in the inner tube has an opposite behavior. The maximum amplitude of the shear stress τ_{13} increases with an increase in both ϵ and δ as displayed in Figure 13. Figure 14 shows that there is no variation in the shear stress τ_{13} along the annulus in the case of solid wall annulus ($\phi = 0$), but an apparent variation is noticed at $\phi > 0$ (peristaltic movement). The figure also shows that, in the peristaltic movement case ($\phi > 0$), there is an apparent variation in the shear stress τ_{13} with various values
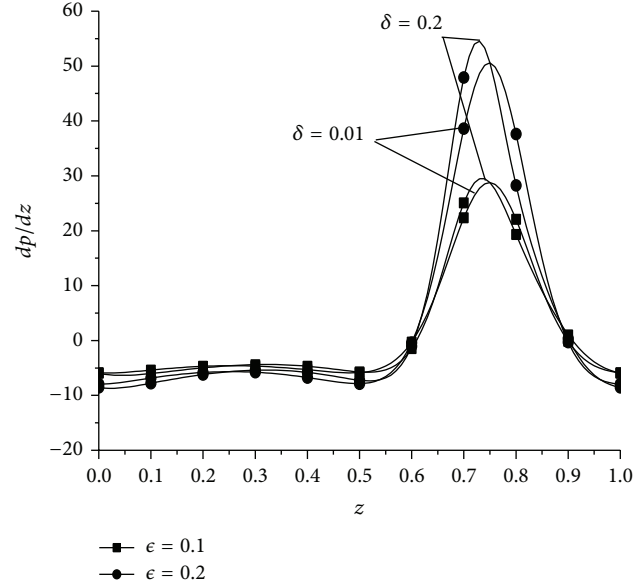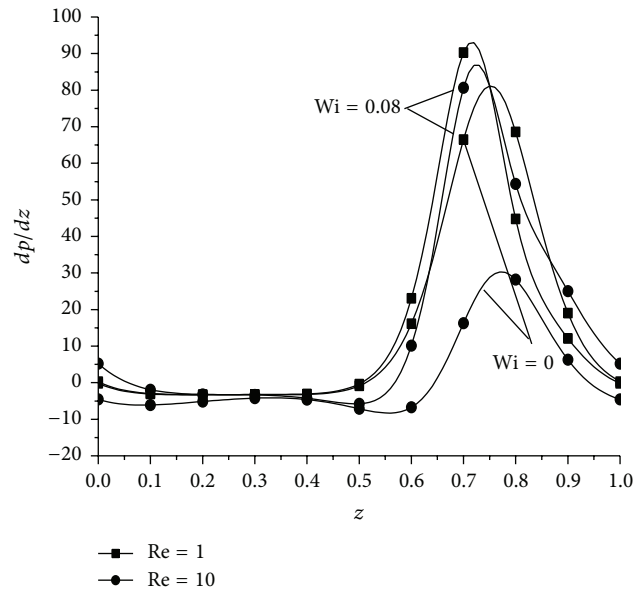
of the Weissenberg number Wi along the annulus. The inverse results are seen through Figures 15 and 16 for the shear stress at the inner wall.

7.3. Trapping Phenomenon. An important phenomenon in peristaltic motion is trapping. In a wave frame, the streamline under particular conditions split to trap a bolus which moves as a whole with the speed of the peristaltic wave. The effects of the Reynolds number Re, Weissenberg parameter Wi, the wave number δ, and radius ratio ϵ on trapping can be observed through Figures 17, 18, 19, and 20. The effect of
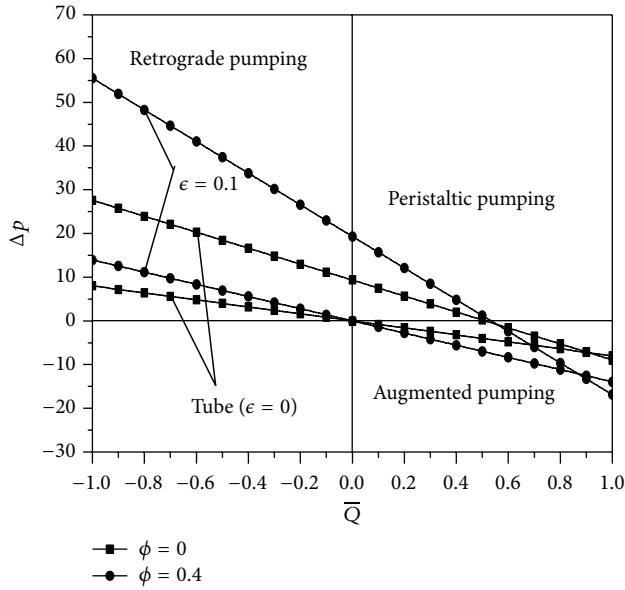
FIGURE 12: The variation of pressure rise over the length Δp with $\overline{Q}$ for different values of ϕ and ϵ at Wi = 0.01, Re = 10, and $\delta = 0.08$.
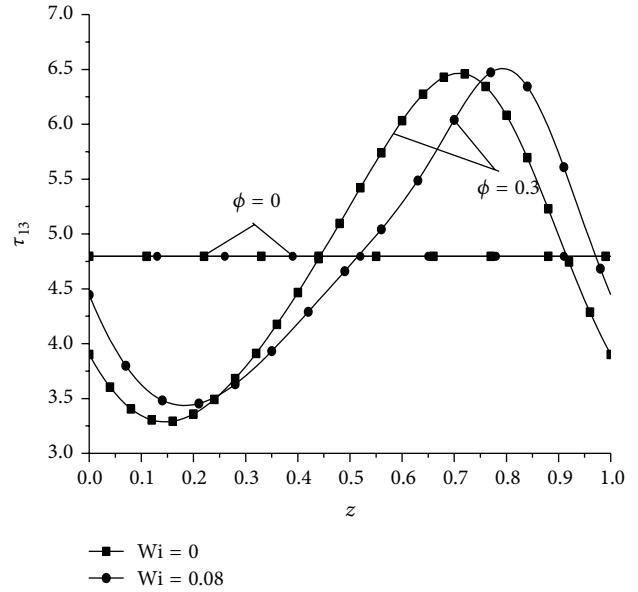

FIGURE 14: Wall shear stress τ_{13} at the outer wall versus z with different values of ϕ and Wi at $\epsilon = 0.1$, $\overline{Q} = 1$, $\delta = 0.08$, and Re = 10.
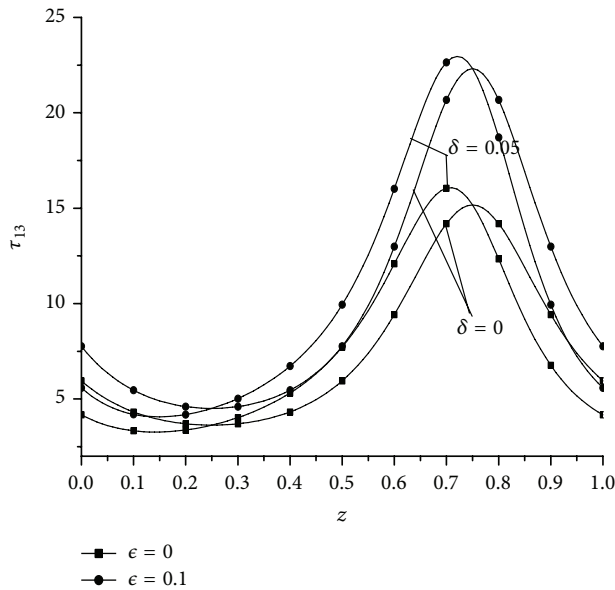

FIGURE 13: Wall shear stress τ_{13} at the outer wall versus z with different values of δ and ϵ at Wi = 0.01, $\overline{Q} = 1.5$, $\phi = 0.4$, and Re = 10.
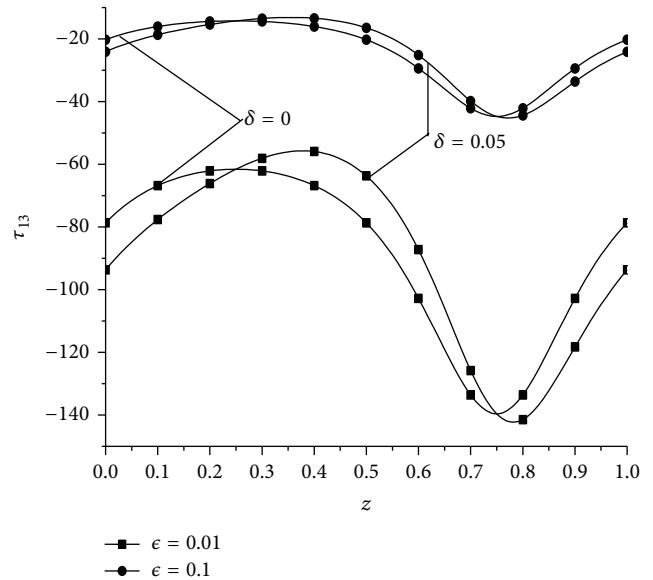
FIGURE 15: Wall shear stress τ_{13} at the inner wall versus z with different values of δ and ϵ at Wi = 0.01, $\overline{Q} = 1.5$, $\phi = 0.4$, and Re = 10.

inertia on trapping is shown in Figure 17. The figure displays that the streamlines corresponding to Re = 0 in Figure 17(a) are in the form of trapped bolus and by elevating the values of Re more trapped boluses appear as in Figure 17(b). With further increase in Re, we find the presence of a second eddy as seen in Figure 17(c). We can see that there is no substantial difference to be seen on trapping by changing Weissenberg parameter Wi as shown in Figure 18. In order to see the effect of the curvature δ on trapping we have plotted Figure 19. We see that the shape of the trapped bolus is deformed by

increasing the values of the dimensionless wave number δ. The streamlines graph for different values of radius ratio ϵ is plotted in Figure 19. The "trapping" phenomena occur for $\epsilon = 0.2$ (Figure 19(a)). But for a further decrease in ($\epsilon = 0$) (tube), the trapped bolus is seen with large size and the trapping range increases gradually as in Figure 19(c).

8. Concluding Results

The mathematical model of peristaltic transport of flow in a gap between two coaxial tubes filled with Maxwell fluid is
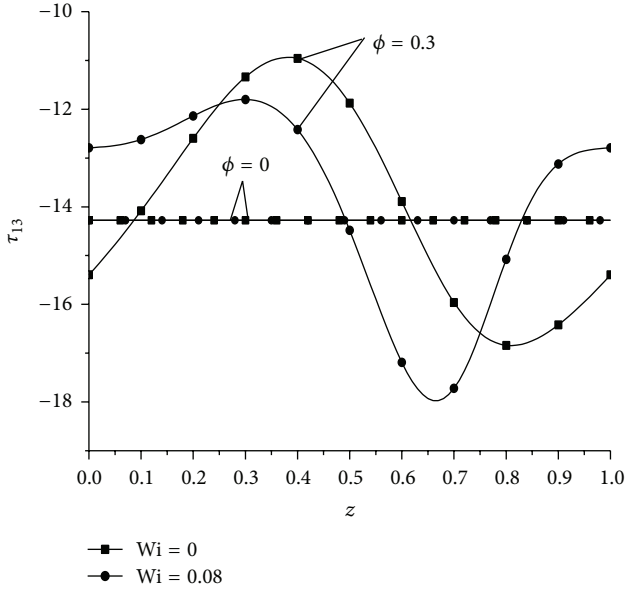
FIGURE 16: Wall shear stress τ_{13} at the inner wall versus z with different values of ϕ and Wi at $\epsilon = 0.1, \overline{Q} = 1, \delta = 0.08$, and Re $= 10$.

studied analytically. The main findings can be summarized as follows.

   (i) There exist two values of a separation points at the outer wall of the annulus. An important result is that there is no separation when $\phi = 0$ (solid wall) on both the tube wall and the annulus walls. Moreover, the separation points are different in the tube than those in the annulus.

   (ii) In the narrow part of the annulus, the maximum amplitude of the pressure gradient for Maxwell fluid is different from the Newtonian fluid.

   (iii) Inertial force effect on the peristaltic flow is stronger for the case of larger amplitude ratio.

   (iv) The shear stress τ_{13} in the outer tube along the annulus varies from small values in the wider part to large values in the narrow part, but the shear stress in the inner tube behaves oppositely.

   (v) The presence of the endoscope tube ($\epsilon \neq 0$) in an artery increases the pressure gradient and shear stress. Such a result seems reasonable from the physical and medical point of view.

   (vi) The presence of a second eddy is seen by increasing the values of the Reynolds number.

Appendix

$$\Omega_1 = 2r_2\left(\epsilon^2 - r_2^2\right)\left(\epsilon^2\left(-1 + \log[\epsilon] - \log[r_2]\right)\right.$$
$$\left. + r_2^2\left(1 + \log[\epsilon] - \log[r_2]\right)\right)$$
$$\times \left(\log[\epsilon] - \log[r_2]\right),$$

$$\Omega_2 = 2\epsilon^2 r_2^2 + \epsilon^4\left(-1 + \log[\epsilon] - \log[r_2]\right)$$
$$+ r_2^4\left(-1 - \log[\epsilon] + \log[r_2]\right),$$

$$\Omega_3 = \left(\epsilon\left(F_0 - \epsilon^2 + r_2^2\right)\right.$$
$$\times \left(\epsilon^2 + r_2^2\left(-1 - 2\log[\epsilon] + 2\log[r_2]\right)\right)r_2'\right)$$
$$\times \left(\Omega_1\right)^{-1},$$

$$\Omega_4 = \left(\left(F_0 - \epsilon^2 + r_2^2\right)\right.$$
$$\times \left(\epsilon^2 + r_2^2\left(-1 - 2\log[\epsilon] + 2\log[r_2]\right)\right)r_2'\right)$$
$$\times \left(\Omega_1\right)^{-1},$$

$$\Omega_5 = \left(2\left(F_0 - \epsilon^2 + r_2^2\right)\right.$$
$$\times \left(\epsilon^2 + r_2^2\left(-1 - 2\log[\epsilon] + 2\log[r_2]\right)\right)r_2'\right)$$
$$\times \left(\Omega_1\right)^{-1},$$

$$\Omega_6 = \left(2\left(F_0 - \epsilon^2 + r_2^2\right)\log[\epsilon]\right.$$
$$\times \left(\epsilon^2 + r_2^2\left(-1 - 2\log[\epsilon] + 2\log[r_2]\right)\right)r_2'\right)$$
$$\times \left(\Omega_1\right)^{-1},$$

$$\Omega_7 = \left(-\frac{2\epsilon^2\left(F_0 - \epsilon^2 + r_2^2\right)}{\Omega_2} + \frac{2r_2^2\left(F_0 - \epsilon^2 + r_2^2\right)}{\Omega_2}\right),$$

$$\Omega_8 = \frac{2\epsilon^2\left(F_0 - \epsilon^2 + r_2^2\right)\log[r_2]}{\Omega_2}$$
$$- \frac{2r_2^2\left(F_0 - \epsilon^2 + r_2^2\right)\log[\epsilon]}{\Omega_2},$$

$$\Omega_9 = \frac{2\left(F_0 - \epsilon^2 + r_2^2\right)\left(\log[\epsilon] - \log[r_2]\right)}{\Omega_2},$$

$$\Omega_{10} = 2\mathrm{Wi}\Omega_4\Omega_7 + 2\mathrm{Wi}\Omega_6\Omega_7,$$

$$\Omega_{11} = 4\mathrm{Wi}\Omega_3\Omega_9 - 4\mathrm{Wi}\Omega_4\Omega_9$$
$$+ 4\mathrm{Wi}\Omega_5\Omega_9 - 4\mathrm{Wi}\Omega_6\Omega_9,$$

$$\Omega_{12} = \mathrm{Wi}\Omega_8\Omega_7' - \mathrm{Wi}\Omega_7',$$

$$\Omega_{13} = -4\mathrm{Wi}\Omega_4\Omega_9 - 4\mathrm{Wi}\Omega_6\Omega_9 + \mathrm{Wi}\Omega_9\Omega_7'$$
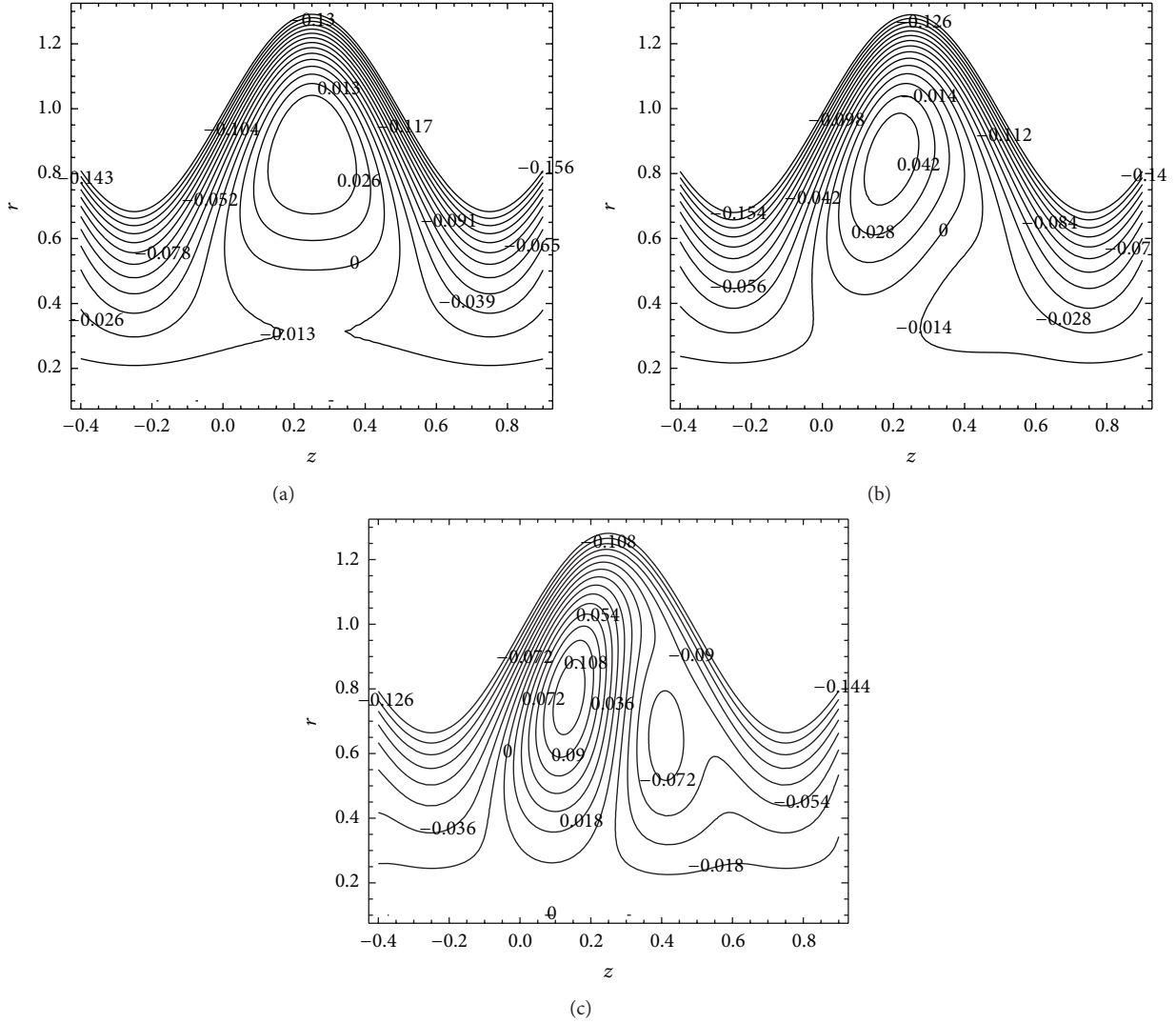$$- 2\mathrm{Wi}\Omega_9' + 2\mathrm{Wi}\Omega_8\Omega_9',$$

(a)

(b)

(c)

FIGURE 17: The effect of Reynolds number on the streamline patterns in the wave frame for different three values of Re: (a) Re = 0, (b) Re = 10, (c) Re = 50 at Wi = 0.02, $\epsilon = 0.1$, $\overline{Q} = 0.7$, $\delta = 0.156$, and $\phi = 0.3$, $r \in [\epsilon, r_2]$.

$$\Omega_{14} = \left(2\Omega_5\Omega_9 + \Omega_7\Omega_9'\right),$$

$$\Omega_{15} = -\Omega_{10} + 4\mathrm{Wi}\Omega_5\Omega_7,$$

$$\Omega_{16} = \Omega_{11} + \mathrm{Re}\,\Omega_3\Omega_7 - 4\mathrm{Wi}\Omega_5\Omega_9,$$

$$\Omega_{17} = \frac{\Omega_{13}}{2} - \frac{1}{2}\mathrm{Wi}\Omega_{14} - \frac{1}{4}\mathrm{Re}\,\Omega_4\Omega_7$$

$$- \frac{1}{4}\mathrm{Re}\,\Omega_5\Omega_7 - \frac{1}{4}\mathrm{Re}\,\Omega_6\Omega_7$$

$$+ \frac{1}{4}\mathrm{Re}\,\Omega_7' + \frac{3}{8}\mathrm{Re}\,\Omega_7\Omega_7' - \frac{1}{4}\mathrm{Re}\,\Omega_8\Omega_7'$$

$$- \frac{1}{4}\mathrm{Re}\,\Omega_8' - \frac{1}{4}\mathrm{Re}\,\Omega_7\Omega_8' + \frac{1}{4}\mathrm{Re}\,\Omega_8\Omega_8',$$

$$\Omega_{18} = \mathrm{Wi}\Omega_{14} + \frac{1}{4}\mathrm{Re}\,\Omega_5\Omega_7 - \frac{1}{4}\mathrm{Re}\,\Omega_7'$$

$$- \frac{1}{2}\mathrm{Re}\,\Omega_7\Omega_7' + \frac{1}{4}\mathrm{Re}\,\Omega_8\Omega_7' + \frac{1}{4}\mathrm{Re}\,\Omega_7\Omega_8',$$

$$\Omega_{19} = -\frac{1}{8}\mathrm{Re}\,\Omega_4\Omega_9 - \frac{1}{16}\mathrm{Re}\,\Omega_5\Omega_9 - \frac{1}{8}\mathrm{Re}\,\Omega_6\Omega_9$$

$$- \frac{1}{32}\mathrm{Re}\,\Omega_9\Omega_7' + \frac{1}{16}\mathrm{Re}\,\Omega_9\Omega_8' - \frac{1}{16}\mathrm{Re}\,\Omega_9'$$

$$- \frac{1}{32}\mathrm{Re}\,\Omega_7\Omega_9' + \frac{1}{16}\mathrm{Re}\,\Omega_8\Omega_9' + \frac{1}{2}\mathrm{Wi}\Omega_9\Omega_9',$$

$$\Omega_{20} = \left(\frac{1}{8}\mathrm{Re}\,\Omega_5\Omega_9 + \frac{1}{16}\mathrm{Re}\,\Omega_9\Omega_7' + \frac{1}{16}\mathrm{Re}\,\Omega_7\Omega_9'\right),$$

$$\Omega_{21} = -\epsilon^2\Omega_{17} - \frac{\epsilon^2\log[\epsilon]\,\Omega_{17}}{-\log[\epsilon] + \log[r_2]}$$

$$+ \frac{r_2^2\log[\epsilon]\,\Omega_{17}}{-\log[\epsilon] + \log[r_2]} - \epsilon^2\log[\epsilon]\,\Omega_{18}$$

(a)

(b)

(c)
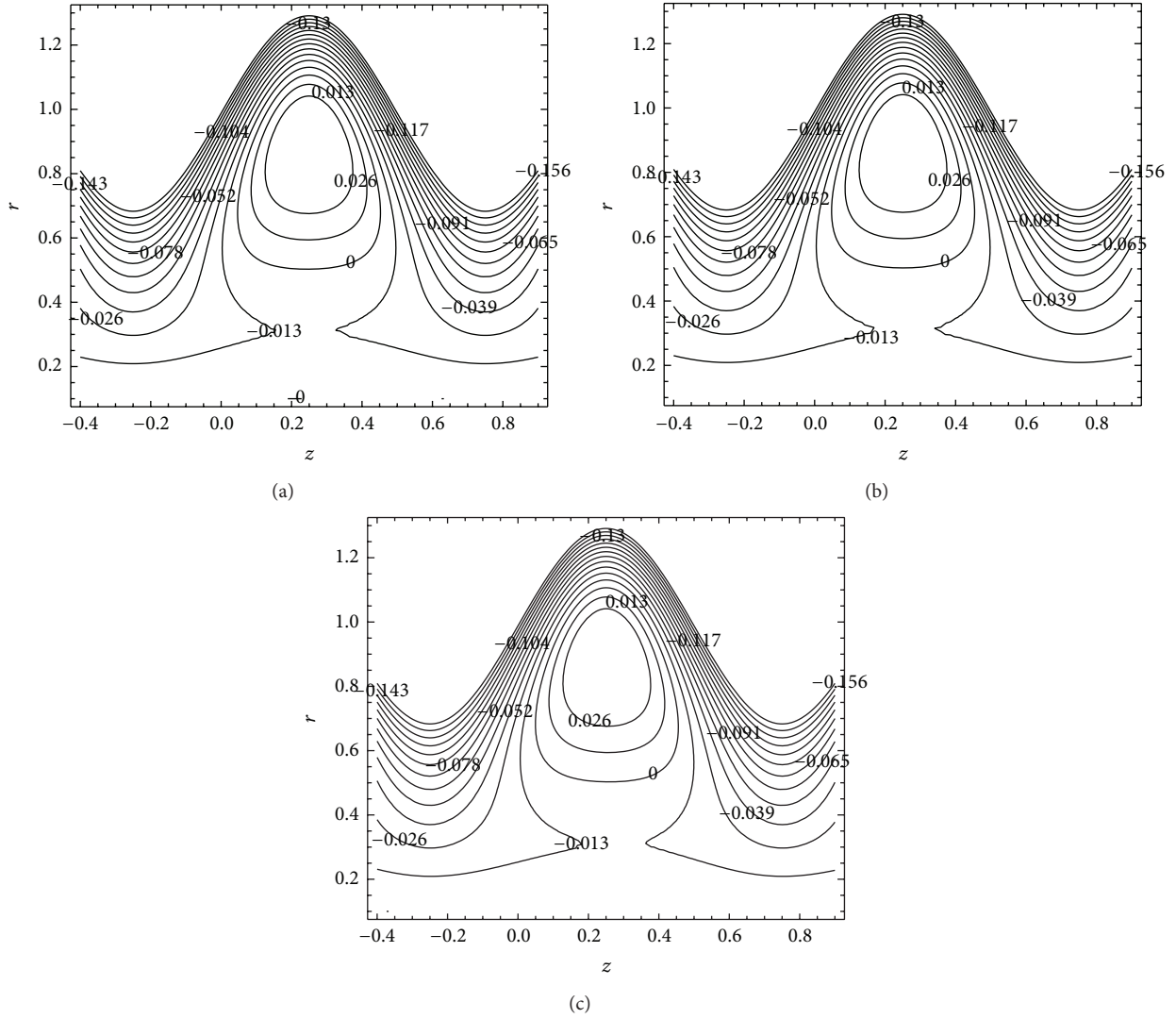
Figure 18: Graph of streamlines for different three values of Wi: (a) Wi = 0, (b) Wi = 0.04, (c) Wi = 0.08 at $\epsilon = 0.1$, $\overline{Q} = 0.7$, $\delta = 0.156$, Re = 0.1, and $\phi = 0.3$, $r \in [\epsilon, r_2]$.

$$-\frac{\epsilon^2 \log[\epsilon]^2 \Omega_{18}}{-\log[\epsilon] + \log[r_2]} + \frac{r_2^2 \log[\epsilon] \log[r_2] \Omega_{18}}{-\log[\epsilon] + \log[r_2]}$$

$$-\epsilon^4 \left(\Omega_{19} + \log[\epsilon] \Omega_{20}\right)$$

$$-\frac{\epsilon^4 \log[\epsilon] \left(\Omega_{19} + \log[\epsilon] \Omega_{20}\right)}{-\log[\epsilon] + \log[r_2]}$$

$$+\frac{r_2^4 \log[\epsilon] \left(\Omega_{19} + \log[r_2] \Omega_{20}\right)}{-\log[\epsilon] + \log[r_2]}$$

$$-\frac{\Omega_{15} + 2\mathrm{Wi} \log[\epsilon] \Omega_5 \Omega_7}{\epsilon}$$

$$-\frac{\log[\epsilon] \left(\Omega_{15} + 2\mathrm{Wi} \log[\epsilon] \Omega_5 \Omega_7\right)}{\epsilon \left(-\log[\epsilon] + \log[r_2]\right)}$$

$$+\frac{\log[\epsilon] \left(\Omega_{15} + 2\mathrm{Wi} \log[r_2] \Omega_5 \Omega_7\right)}{r_2 \left(-\log[\epsilon] + \log[r_2]\right)}$$

$$-\frac{2}{9} \mathrm{Re}\, \epsilon^3 \Omega_3 \Omega_9 - \frac{2\,\mathrm{Re}\, \epsilon^3 \log[\epsilon] \Omega_3 \Omega_9}{9\left(-\log[\epsilon] + \log[r_2]\right)}$$

$$+\frac{2\,\mathrm{Re}\, r_2^3 \log[\epsilon] \Omega_3 \Omega_9}{9\left(-\log[\epsilon] + \log[r_2]\right)}$$

$$-\epsilon \left(\Omega_{16} + 4\mathrm{Wi} \log[\epsilon] \Omega_5 \Omega_9\right)$$

$$-\frac{\epsilon \log[\epsilon] \left(\Omega_{16} + 4\mathrm{Wi} \log[\epsilon] \Omega_5 \Omega_9\right)}{-\log[\epsilon] + \log[r_2]}$$

$$+\frac{r_2 \log[\epsilon] \left(\Omega_{16} + 4\mathrm{Wi} \log[r_2] \Omega_5 \Omega_9\right)}{-\log[\epsilon] + \log[r_2]}$$
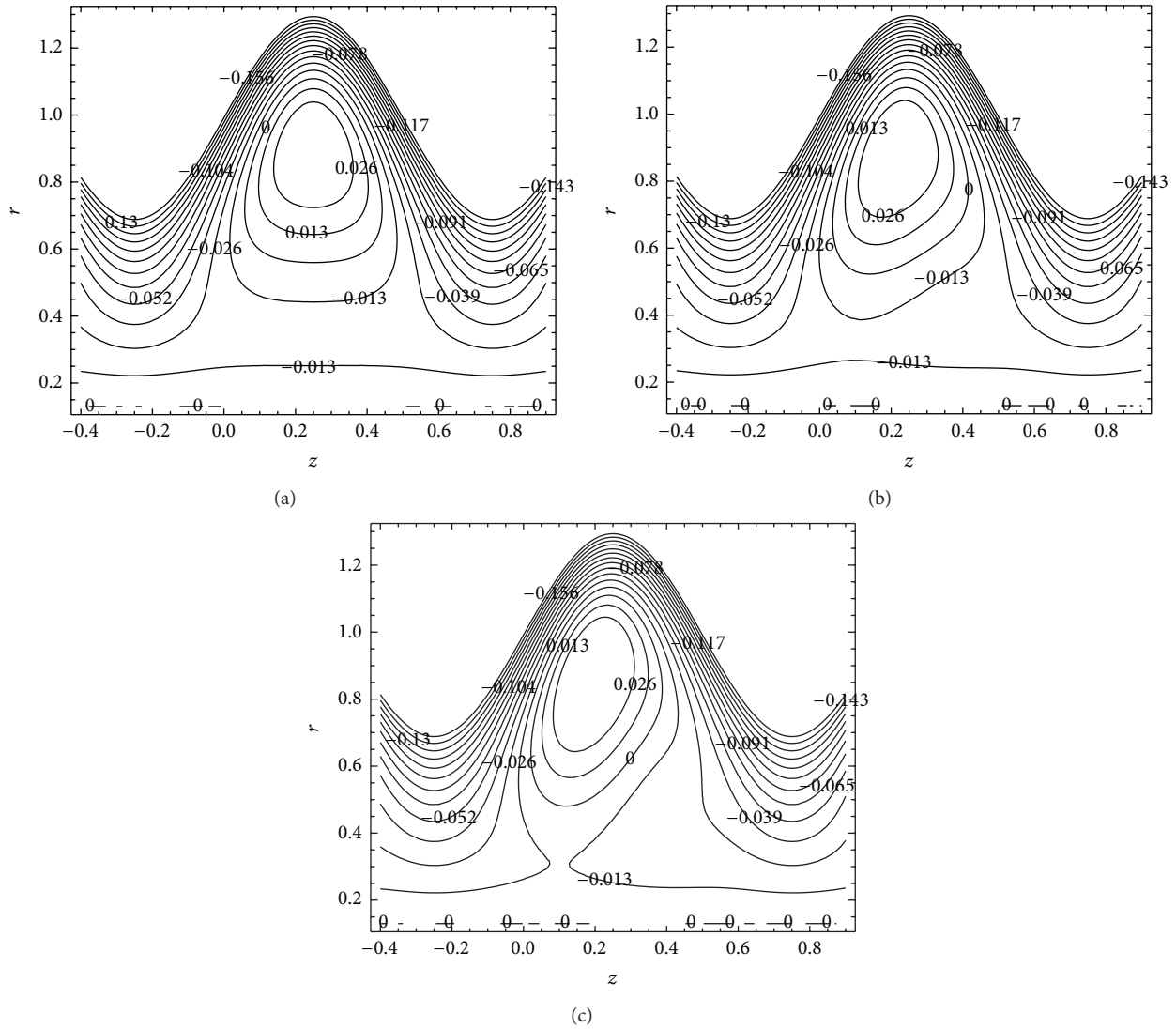
(a)

(b)

(c)

Figure 19: Graph of streamlines for different three values of δ: (a) $\delta = 0$, (b) $\delta = 0.08$, (c) $\delta = 0.156$ at $\epsilon = 0.13$, $\overline{Q} = 0.7$, Wi = 0.05, Re = 10, and $\phi = 0.3$, $r \in [\epsilon, r_2]$.

$$- \frac{1}{2} \text{Wi} \log [\epsilon]^2 \Omega_7 \Omega_7'$$

$$- \frac{1}{4} \text{Re} \, \epsilon^2 \log [\epsilon]^2 \Omega_7 \Omega_7'$$

$$- \frac{\text{Wi} \log [\epsilon]^3 \Omega_7 \Omega_7'}{2 \left(- \log [\epsilon] + \log [r_2] \right)}$$

$$- \frac{\text{Re} \, \epsilon^2 \log [\epsilon]^3 \Omega_7 \Omega_7'}{4 \left(- \log [\epsilon] + \log [r_2] \right)}$$

$$+ \frac{\text{Wi} \log [\epsilon] \log [r_2]^2 \Omega_7 \Omega_7'}{2 \left(- \log [\epsilon] + \log [r_2] \right)}$$

$$+ \frac{\text{Re} \, r_2^2 \log [\epsilon] \log [r_2]^2 \Omega_7 \Omega_7'}{4 \left(- \log [\epsilon] + \log [r_2] \right)} - \frac{1}{36} \text{Re} \, \epsilon^6 \Omega_9 \Omega_9'$$

$$- \frac{\text{Re} \, \epsilon^6 \log [\epsilon] \, \Omega_9 \Omega_9'}{36 \left(- \log [\epsilon] + \log [r_2] \right)}$$

$$+ \frac{\text{Re} \, r_2^6 \log [\epsilon] \, \Omega_9 \Omega_9'}{36 \left(- \log [\epsilon] + \log [r_2] \right)},$$

$$\Omega_{22} = - \frac{1}{- \log [\epsilon] + \log [r_2]}$$

$$\times \left(- \epsilon^2 \Omega_{17} + r_2^2 \Omega_{17} - \epsilon^2 \log [\epsilon] \, \Omega_{18} \right.$$

$$+ r_2^2 \log [r_2] \, \Omega_{18} - \epsilon^4 \left(\Omega_{19} + \log [\epsilon] \, \Omega_{20} \right)$$

$$+ r_2^4 \left(\Omega_{19} + \log [r_2] \, \Omega_{20} \right)$$

$$- \frac{\Omega_{15} + 2 \text{Wi} \log [\epsilon] \, \Omega_5 \Omega_7}{\epsilon}$$
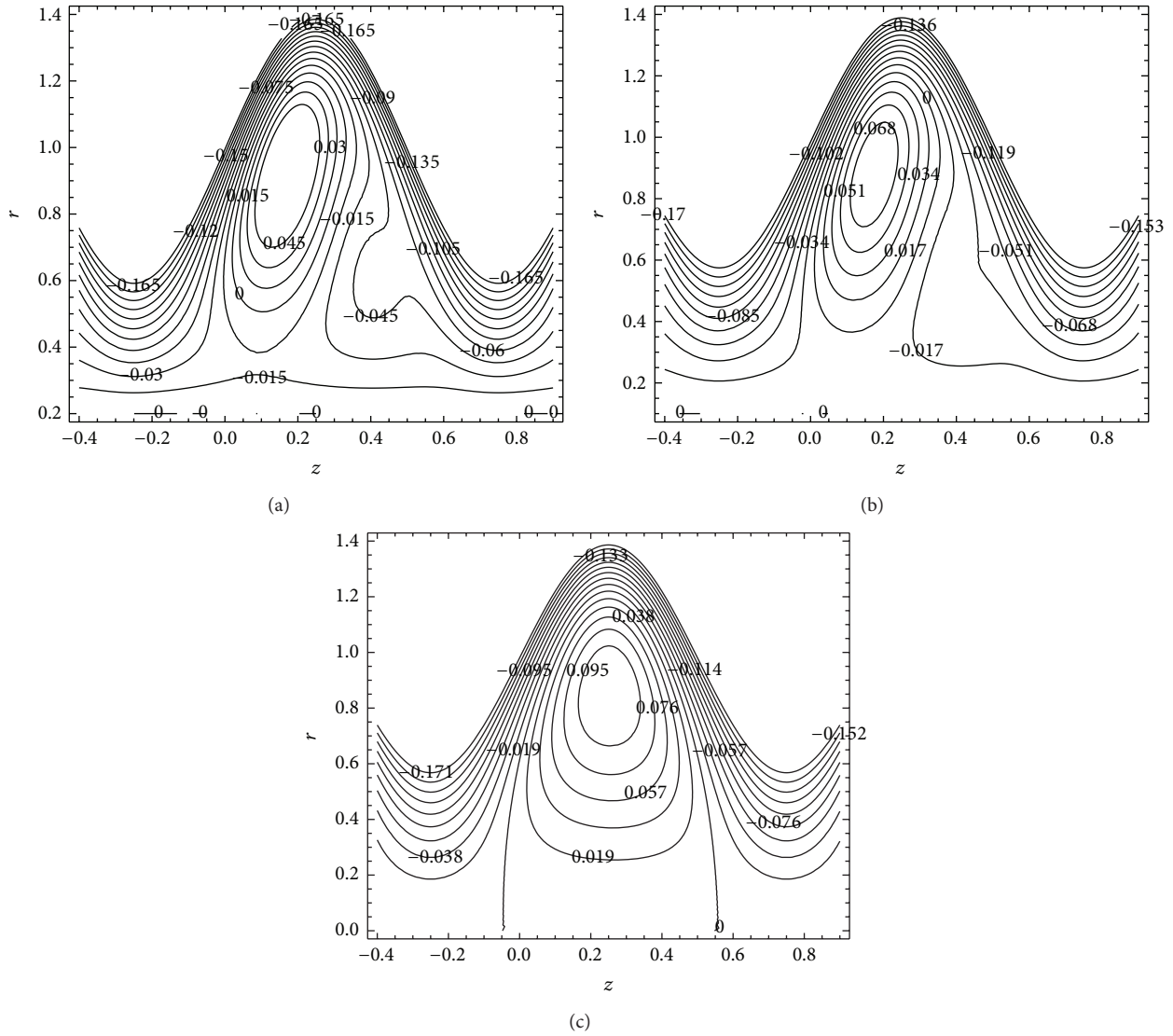
(a)

(b)

(c)

Figure 20: Graph of streamlines for different three values of ϵ: (a) $\epsilon = 0.2$, (b) $\epsilon = 0.1$, (c) $\epsilon = 0.0$ at $\delta = 0.156$, $\overline{Q} = 0.7$, Wi $= 0.05$, Re $= 15$, and $\phi = 0.4$, $r \in [\epsilon, r_2]$.

$$+ \frac{\Omega_{15} + 2\text{Wi} \log [r_2] \Omega_5 \Omega_7}{r_2}$$

$$- \frac{2}{9} \text{Re} \, \epsilon^3 \Omega_3 \Omega_9 + \frac{2}{9} \text{Re} \, r_2^3 \Omega_3 \Omega_9$$

$$- \epsilon \left(\Omega_{16} + 4\text{Wi} \log [\epsilon] \Omega_5 \Omega_9 \right)$$

$$+ r_2 \left(\Omega_{16} + 4\text{Wi} \log [r_2] \Omega_5 \Omega_9 \right)$$

$$- \frac{1}{2} \text{Wi} \log [\epsilon]^2 \Omega_7 \Omega_7'$$

$$- \frac{1}{4} \text{Re} \, \epsilon^2 \log [\epsilon]^2 \Omega_7 \Omega_7'$$

$$+ \frac{1}{2} \text{Wi} \log [r_2]^2 \Omega_7 \Omega_7'$$

$$+ \frac{1}{4} \text{Re} \, r_2^2 \log [r_2]^2 \Omega_7 \Omega_7' - \frac{1}{36} \text{Re} \, \epsilon^6 \Omega_9 \Omega_9'$$

$$\left. + \frac{1}{36} \text{Re} \, r_2^6 \Omega_9 \Omega_9' \right),$$

$$c_6 = -\frac{1}{\epsilon} \left[-\frac{1}{36} \epsilon^6 \left(6\Omega_{19}' - \Omega_{20}' \right) \right.$$

$$- \epsilon \left(\Omega_{15}' - 2\text{Wi} \left(\Omega_7 \Omega_5' + \Omega_5 \Omega_7' \right) \right)$$

$$- \frac{2}{45} \text{Re} \, \epsilon^5 \left(\Omega_9 \Omega_3' + \Omega_3 \Omega_9' \right)$$

$$- \frac{1}{9} \epsilon^3 \left(3\Omega_{16}' - 4\text{Wi} \left(\Omega_9 \Omega_5' + \Omega_5 \Omega_9' \right) \right)$$

$$- \frac{1}{16} \epsilon^2 \left(4\text{Wi} + \text{Re} \, \epsilon^2 \right) \log [\epsilon]^2 \left(\Omega_7'^2 + \Omega_7 \Omega_7'' \right)$$

$$- \frac{1}{128} \epsilon^4 \left(32 \Omega_{17}' - 8 \Omega_{18}' + \text{Re} \left(\Omega_7'^2 + \Omega_7 \Omega_7'' \right) \right)$$

$$- \frac{\epsilon^2}{\left(16 r_2 (\log (\epsilon / r_2))^2 \right)}$$

$$\times \left(\frac{dp_1}{dz} \left(1 + 2 \log [\epsilon] \right) \right.$$

$$\times \left(\epsilon^2 + r_2^2 \left(-1 - 2 \log \frac{\epsilon}{r_2} \right) \right) r_2'$$

$$+ 2 r_2 \left(\log \frac{\epsilon}{r_2} \right)^2$$

$$\left. \times \left(4 \Omega_{21}' - 2 \Omega_{22}' + \text{Wi} \left(\Omega_7'^2 + \Omega_7 \Omega_7'' \right) \right) \right)$$

$$- \frac{\log [\epsilon]}{\left(8 r_2 (\log (\epsilon / r_2))^2 \right)}$$

$$\times \left(\frac{1}{6} \epsilon^6 \Omega_{20}' + 2 \text{Wi} \epsilon \left(\Omega_7 \Omega_5' + \Omega_5 \Omega_7' \right) \right.$$

$$+ \frac{4}{3} \text{Wi} \epsilon^3 \left(\Omega_9 \Omega_5' + \Omega_5 \Omega_9' \right)$$

$$+ \frac{\epsilon^4}{32} \epsilon^4 \left(8 \Omega_{18}' - \text{Re} \left(\Omega_7'^2 + \Omega_7 \Omega_7'' \right) \right)$$

$$+ \left(\epsilon^2 \left(\frac{dp_1}{dz} \left(-\epsilon^2 + r_2^2 \left(1 + 2 \log \frac{\epsilon}{r_2} \right) \right) r_2' \right. \right.$$

$$+ 2 r_2 \left(\log \frac{\epsilon}{r_2} \right)^2$$

$$\times \left(2 \Omega_{22}' \right.$$

$$\left. \left. \left. \left. - \text{Wi} \left(\Omega_7'^2 + \Omega_7 \Omega_7'' \right) \right) \right) \right) \right)$$

$$\left. - \frac{1}{288} \text{Re} \, \epsilon^8 \left(\Omega_9'^2 + \Omega_9 \Omega_9'' \right) \right].$$

$$(\text{A.1})$$

Conflict of Interests

The authors declare that they have no conflict of interests regarding the publication of this paper.

Acknowledgments

References

[1] T. W. Latham, *Fluid motion in a peristaltic pump [M.Sc. thesis]*, Massachusetts Institute of Technology, Cambridge, Mass, USA, 1966.

[2] A. H. Shapiro, M. Y. Jaffrin, and S. L. Weinberg, "Peristaltic pumping with long wavelength at low Reynolds number," *Journal of Fluid Mechanics*, vol. 37, no. 4, pp. 799–825, 1969.

[3] T. F. Zien and S. A. Ostrach, "A long wave approximation to peristaltic motion," *Journal of Biomechanics*, vol. 3, no. 1, pp. 63–75, 1970.

[4] R. A. Ramachandra and S. Usha, "Peristaltic transport of two immiscible viscous fluids in a circular tube," *Journal of Fluid Mechanics*, vol. 298, pp. 271–285, 1995.

[5] Kh. S. Mekheimer, E. F. El Shehawey, and A. M. Elaw, "Peristaltic motion of a particle-fluid suspension in a planar channel," *International Journal of Theoretical Physics*, vol. 37, no. 11, pp. 2895–2920, 1998.

[6] R. B. Bird, R. G. Armstrong, and O. Hassager, *Dynamics of Polymeric Liquids, Fluid Mechanics*, vol. 1, John Wiley & Sons, New York, NY, USA, 1987.

[7] J. G. Oldroyd, "On the formulation of rheological equations of state," *Proceedings of the Royal Society of London A: Mathematical, Physical and Engineering Sciences*, vol. 200, pp. 523–541, 1950.

[8] T. Hayat, A. Afsar, M. Khan, and S. Asghar, "Peristaltic transport of a third order fluid under the effect of a magnetic field," *Computers & Mathematics with Applications*, vol. 53, no. 7, pp. 1074–1087, 2007.

[9] Y. Abd elmaboud and Kh. S. Mekheimer, "Non-linear peristaltic transport of a second-order fluid through a porous medium," *Applied Mathematical Modelling*, vol. 35, no. 6, pp. 2695–2710, 2011.

[10] A. E. H. Abd El Naby, A. E. M. El Misery, and M. F. Abd El Kareem, "Effects of a magnetic field on trapping through peristaltic motion for generalized Newtonian fluid in channel," *Physica A: Statistical Mechanics and Its Applications*, vol. 367, pp. 79–92, 2006.

[11] T. Hayat, M. Khan, A. M. Siddiqui, and S. Asghar, "Non-linear peristaltic flow of a non-Newtonian fluid under effect of a magnetic field in a planar channel," *Communications in Nonlinear Science and Numerical Simulation*, vol. 12, no. 6, pp. 910–919, 2007.

[12] D. Tsiklauri and I. Beresnev, "Non-Newtonian effects in the peristaltic flow of a Maxwell fluid," *Physical Review E*, vol. 64, no. 2, part 2, Article ID 036303, 2001.

[13] Kh. S. Mekheimer and A. N. Abdel-Wahab, "Net annulus flow of a compressible viscous liquid with peristalsis," *Journal of Aerospace Engineering*, vol. 25, no. 4, pp. 660–669, 2012.

[14] A. M. Siddiqui and W. H. Schwarz, "Peristaltic flow of a second-order fluid in tubes," *Journal of Non-Newtonian Fluid Mechanics*, vol. 53, pp. 257–284, 1994.

[15] Kh. S. Mekheimer and A. N. Abdel-Wahab, "Compressibility effects on peristaltic flow of a non-Newtonian Maxwell fluid through an annulus," in *Fluid Transport: Theory, Dynamics and Transport*, pp. 219–235, Nova Science Publishers, 2011.

[16] K. Vajravelu, S. Sreenadh, and V. R. Babu, "Peristaltic transport of a Herschel—Bulkley fluid in an inclined tube," *International Journal of Non-Linear Mechanics*, vol. 40, no. 1, pp. 83–90, 2005.

[17] A. V. Mernone and J. N. Mazumdar, "A mathematical study of peristaltic transport of a casson fluid," *Mathematical and Computer Modelling*, vol. 35, no. 7-8, pp. 895–912, 2002.

[18] Kh. S. Mekheimer, "Peristaltic transport of a Newtonian fluid through a uniform and non-uniform annulus," *The Arabian Journal for Science and Engineering*, vol. 30, no. 1A, p. 69, 2005.

[19] A. E. H. Abd El Naby and A. E. M. El Misiery, "Effects of an endoscope and generalized Newtonian fluid on peristaltic motion," *Applied Mathematics and Computation*, vol. 128, no. 1, pp. 19–35, 2002.

[20] A. E. H. Abd El Naby, A. E. M. El Misery, and I. I. El Shamy, "Effects of an endoscope and fluid with variable viscosity on peristaltic motion," *Applied Mathematics and Computation*, vol. 158, no. 2, pp. 497–511, 2004.

[21] T. Hayat, N. Ali, S. Asghar, and A. M. Siddiqui, "Exact peristaltic flow in tubes with an endoscope," *Applied Mathematics and Computation*, vol. 182, no. 1, pp. 359–368, 2006.

[22] Kh. S. Mekheimer and Y. Abd Elmaboud, "Peristaltic flow through a porous medium in an annulus: application of an endoscope," *Applied Mathematics & Information Sciences*, vol. 2, no. 1, pp. 103–121, 2008.

[23] A. Chorin and J. Marsden, *A Mathematical Introduction to Fluid Mechanics*, Springer, New York, NY, USA, 1997.

[24] R. L. Burden and J. D. Faires, *Numerical Analysis*, Brooks Cole, Florence, Ky, USA, 9th edition, 2010.